Out-of-plane displacement derivative measurement: comparison of results obtained by a shearographic interferometer using the separation of the polarization states and the finite element method

Vanessa Rosso[1*], Lihong Zhang[2], Fabrice Michel[1], Yvon Renotte[1],
Yves Lion[1], Anne-Marie Habraken[2]

[1]HOLOLAB, Department of Physics, Bat. B5a, Université de Liège, B-4000 Liège, Belgium.
[2]Mechanics of Materials and Structures (M&S) Department, Bat. B52, Université de Liège, B-4000 Liège, Belgium.

ABSTRACT

An original experimental setup for shearography with metrological applications is presented herein. The simplicity and the efficiency of the setup are provided by a shearing device, a prism that separates the TE and TM polarization modes with a coating and a thin glass plate attached on its face. The temporal phase shifting method is applied through the use of a liquid crystal variable retarder. The use of this shearing device enables an in-line and almost-common path configuration for the shearing interferometer, a path that leads to high stability of the interferometer and a low sensitivity to external disturbances. In order to prove the efficiency and the accuracy of this speckle shearing interferometer, the out-of-plane displacement derivative relative to the shearing interferometry direction of a centrally loaded steel plate has been measured by the shearographic interferometer and then compared with the out-of-plane displacement derivative computed from the displacement field provided by the finite element method. The results are in good agreement.

Keywords: shearography, speckle interferometry, finite element method, phase-shifting, liquid crystal retarder

1. INTRODUCTION

Over the past few years temporal phase-shifting interferometry, involving techniques such as digital speckle pattern interferometry[1, 2], digital shearography[3], and fringe projection[4], has emerged as a new and efficient technique with non-destructive metrological applications, e.g., three dimensional shape measurement, surface displacement determination and strain field, and vibrational analysis. Shearography, or speckle shearing interferometry, is a full field non-contact optical technique generally used for the measurement of the gradient of the displacement of a mechanically or thermally loaded surface[3, 5-7]. Recent studies have also demonstrated the value of shearography for surface slope and shape measurements[8, 9]. As for any technique based on speckle interferometry, shearography is a useful tool in the micrometer range and can thus complete the nanometric measurement range of holographic interferometry and the macroscopic measurements performed by the fringe projection or stereocorrelation techniques. Extensive work has been reported in this area and, further, different devices for the implementation to shearography of the different types of shear encountered in conventional interferometry have been reported[1-3], some cases are listed hereafter.

Shearing interferometers can be divided into two types, first, those with almost-common optical path interferometers, e.g., those with a glass edge or a Wollaston prism as a shearing device[6, 8], and, second, those that use a Michelson interferometer[10]. In the first group, the two arms corresponding to the object beam and the reference beam are superimposed in one arm. Such a configuration allows the use of a laser with a low coherence length. This feature also makes the almost-common path interferometer less sensitive to external disturbances and, thus, more convenient for industrial uses. However, the sensitivity of typical almost-common path interferometers is limited by the shearing amount that may be imposed by the shearing device, e.g., a birefringent crystal[6, 7] and, as a consequence, it may be

---

[*] Vanessa.Rosso@ulg.ac.be; phone +32 4 3663627 ; fax +32 4 3664516

suitable for only a few applications. In contrast, with the Michelson type interferometer the shearing amount is easily modified[10].

In this work, an original setup for digital phase-shifting shearography is presented. The key element of the experimental setup is the shearing device, a prism with a coating and a thin glass attached plate that separates the two TE and TM polarization modes. This shearing device yields an almost-common path and an in-line configuration of the shearing interferometer, an arrangement that leads to a compact device that is low sensitive to external disturbances. Moreover the sensitivity of the interferometer can be easily modified for different applications by varying the shearing amount with glass plates of different thicknesses or simply by moving the shearing device along the optical axis as proposed by Valera and Jones[11]. Alternatively, the phase shifting method is accomplished by using a liquid crystal variable retarder, which is low cost and permits an easy positioning and a good handiness in the experimental setup relative to other phase shifters such as a piezoelectric translator[2, 3] or a technique using a highly birefringent optical fiber[11, 12],…

Finally in order to validate the efficiency and the accuracy of this shearing interferometer, an experiment consisting in loading centrally a steel plate has been performed and also simulated by the finite element method. The resulting out-of-plane displacement derivative relative to the interferometry shearing direction has been computed from the displacement field provided by the finite element method and compared with the measurements performed by the almost-common path interferometer of shearography. Furthermore a profile of the displacement field computed by the finite element method has been compared with the numerically integrated results experimentally obtained by shearography.

2. DIGITAL PHASE-SHIFTING SHEAROGRAPHY

2.1. Theory

Shearography is a useful tool for measuring the slope contours or the displacement derivatives of an object under a load[3, 5-10]. In order to do so, the optically rough surface of the object to be studied is irradiated with a coherent light to create a speckle pattern. A digital camera (CCD or CMOS) records the interference between this object speckle pattern and an identical speckle pattern spatially displaced, or sheared, thanks to a shearing device; the resulting interferogram is called a shearogram. By comparing the shearograms recorded before and after loading of the object, fringes sensitive to the displacement derivative relative to the shearing direction can be obtained. Phase-shifting[2, 3, 13] and unwrapping[14-16] techniques are usually used to process the phase information from these fringes in order to determine quantitatively the desired metrological parameter. In this study, the general 4-buckets[13] algorithm and the growing region[16] method have been used respectively for phase-shifting and phase unwrapping.

In shearography, the unwrapped phase map, $\Delta_{unwrapped}(x, y)$, obtained thanks to the temporal phase-shifting technique is related to the first derivative of the displacement field relative to the shearing direction X_i of the object speckle wavefront and described in good approximation, when the shearing amount δx_i is small, by the following relationship[3]:

$$\Delta_{unwrapped} = \left[\vec{K} \cdot \vec{e}_X \frac{\partial u}{\partial x_i} + \vec{K} \cdot \vec{e}_Y \frac{\partial v}{\partial x_i} + \vec{K} \cdot \vec{e}_Z \frac{\partial w}{\partial x_i} \right] \delta x_i \tag{1}$$

where $\vec{K}$ is the sensitivity vector of the interferometer, $\vec{e}_X$, $\vec{e}_Y$ and $\vec{e}_Z$ are the unity vectors respectively along the directions X, Y and Z, u, v and w are the components of the displacement vector $\vec{u}$ respectively along the directions X, Y and Z. In this study, the efficiency of the experimental approach is demonstrated for the case of a pure out-of-plane displacement derivative measurement, i.e. the sensitivity vector $\vec{K}$ is orthogonal to the object plane (X, Y). The resulting post-treatment of the phase distribution, $\Delta_{unwrapped}(x, y)$, is then summarized by

$$\Delta_{unwrapped} = \vec{K} \cdot \vec{e}_Z \frac{\partial w}{\partial x_i} \delta x_i \tag{2}$$

The out-of-plane displacement derivative relative to the shearing direction can be determined from Eq. 2.

2.2. The shearing device

The shearing device used in digital shearography splits the light coming from one object point to give two image points in the image plane. A pair of laterally sheared images is thus received by the image sensor. In other words, the shearing device brings light scattered from two neighboring points $P(x, y, z)$ and $P(x+\delta x, y, z)$ on the object surface to interfere at a point on the image plane of a camera. In the present case the shearing is assumed to be parallel to the X-axis and δx is the shearing amount.

Different shearing devices based on the separation of the polarization states are presented in the literature but with those shearing devices, either the shearing amount is fixed[6-8], or the related phase shifting technique is not convenient to be implemented and easily controlled[11, 12].

The key element of this shearing experiment is the shearing prism that separates the two polarization modes. The prism separates an incident wave into two orthogonal linearly polarized waves: a transverse electric, TE, or a s-wave and a transverse magnetic, TM, or a p-wave. The separation of the two polarization states is produced by a coating on the back face of a glass prism obtained from *Edmund Optics*. Theoretically the separation of the polarized states is optimal for a normal incidence on the front face of the prism. In this case the emergent polarized TE and TM waves correspond, respectively, to the beams reflected and transmitted by the coating, see Fig. 1. In order to direct the TE and TM emergent waves in the same direction and to ensure the continuity of the media, a thin glass plate is attached on the coating of the prism with an oil of suitable refractive index, n, in this case 1.522. This glass plate directs by total reflection, the TM polarized wave transmitted by the coating in the same direction as the reflected TE polarized wave. In this way, if the shearing is assumed to be parallel to the X-axis, the TE and TM waves are separated by δx, a distance that is proportional to the thickness of the glass plate, see Fig. 1.
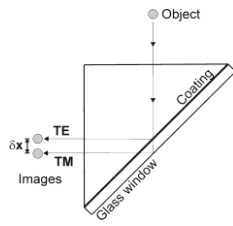

Fig. 1. Schematic of the shearing device using the separation of the polarization states.
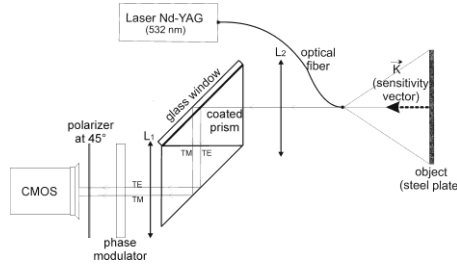
Fig. 2. Experimental setup of the out-of-plane almost-common path interferometer used for shearography.

2.3. The phase modulator: a liquid crystal variable retarder

As with any interferometric technique that uses the temporal phase shifting method, it is necessary to record some interferograms that are phase shifted for comparison with others. In order to produce this phase shift, it is necessary to introduce a phase modulator into the experimental setup. In most of those experiments, a piezoelectric translator (PZT)[2, 3] is used for phase modulation. In contrast, for the interferometric experiments based on the separation of the TE and TM polarization states, the most reported phase modulators[2] are liquid crystal retarders or are based on highly birefringent optical fibers[11, 12]. Contrary to the fiber-based phase modulator, the liquid crystal variable retarder presents the advantages to be very compact and so can be introduce in transmission anywhere in the experimental setup and, moreover, it is less temperature dependent.

When combined with other optical components, liquid crystal variable retarders produce electrically controllable attenuation, linear polarization rotation, or phase modulation. Pure phase modulation is accomplished by aligning the optical axis of the liquid crystal retarder parallel to a linearly polarized input beam. Such a phase modulator uses nematic liquid crystal materials to electrically control polarization. It provides tunable retardation by changing the effective birefringence of the material with an applied voltage.

The calibration of the phase modulator is accomplished by determining the phase shift it induces versus the applied voltage. The liquid crystal variable retarder is well known for exhibiting a high nonlinearity versus the applied voltage and, thus, it has been calibrated in situ following the approach of Ochoa and Huntley[17].

2.4. An almost-common path interferometer for shearography

The design of the experimental setup, which used a pure out-of-plane digital shearography arrangement is illustrated in Fig. 2. The light with a wavelength of 532 nm, comes from a Nd-YAG laser diode with a total output of 30 mW. The object speckle pattern has been produced by retroscattering of the incident light on a test object. The shearograms, recorded by a CMOS camera, arise from the interference between the object speckle wavefront and the same speckle wavefront shifted spatially along the X-axis by the shearing device. The behaviour of the latter has been explained in section 2.2. A second prism has been attached with oil with a refractive index, n, of 1.522 on the shearing device (Fig. 2) in order to make the interferometer compact and in-line. The second prism is a traditional non-polarizing glass prism but is silver coated for better reflectivity; it has the same dimensions as the first shearing prism. In order to produce interference between the two emergent polarized beams, a linear polarizer at 45° relative to the TE and TM polarization directions is introduced in front of the objective of the CMOS camera. A set of four shearograms, phase shifted with respect to one another, have been recorded for a state of the studied object by varying the voltage applied to the liquid crystal variable retarder that has been placed between the second prism and the polarizer at 45°.The slow and fast axes of the phase modulator have been oriented respectively along the TE and TM polarization directions.

Finally, two identical lenses L_1 and L_2 with an effective focal length of 6 cm have been introduced into the experimental setup, see Fig. 2. The role of L_1 is to focus the TM speckle wavefront on the glass-air interface of the shearing device and, consequently, to avoid any variation in the shearing amount as the result of a nonuniform thickness of the thin glass plate. The second lens, L_2, which defocuses the waves, also increases the shearing amount in proportion to its magnification, M_{lens}, and, thus, the shearing amount behind L_2 is

$$\delta x_{lens} = M_{lens} \cdot \delta x \tag{3}$$

In order to simplify the following notation, the value, δx_{lens}, of the shearing amount behind the L_2 lens will simply be referred to as δx.

The shearing amount can be change by replacing the thin glass plate attached to the coating of the prism by another with a different thickness d. On the other hand, according to Eq. 3, the shearing amount varies with the magnification, M_{lens}, that can be modified in moving the shearing device between the two lenses L_1 and L_2, as proposed by Valera and Jones[11].

The resulting experimental setup is an almost-common path interferometer, i.e., the object and reference beams, in shearography the sheared wavefronts, follow almost the same geometric path before interference. Thus, because the two interfering beams would be equally disturbed, this interferometer has the advantage of being less sensitive to external disturbances then do traditional digital speckle interferometers. Moreover, this shearographic interferometer is compact and uses low cost components such as a CMOS camera and a liquid crystal variable retarder compared respectively with an equivalent quality CCD camera and a highly efficient PZT phase shifter.

3. EXPERIMENT

The object to be studied herein is a 282x282x1 mm³ steel plate pierced by three holes in an isosceles triangle arrangement, holes that will become the three points supporting the plate, see Fig. 3. The steel plate has been placed on three balls held by three steel posts screwed into an optical table. A fourth smaller hole is placed at the center of gravity of the isosceles triangle in order to hold, in a reproducible fashion, a ball of known mass, m. The plate is thus centrally loaded and the applied force, F, is equal to the weight of the ball. Only a portion of the steel plate has been scanned by the shearographic interferometer so, in the following, the studied area of the steel plate is a square with a side of 87 mm centered on the load (Fig. 3).

This object-loading system has been chosen to be transportable, reproducible and easily simulated by the finite element method. Three positioning points have been chosen to define univocally the position of the object plane. The X axis defines a symmetry axis, as shown in Fig. 3.a, and consequently, will permit the simulation of half a plate by the finite element method. The behaviour of the complete plate will be reconstructed next by symmetry. The diameters of the holes 1, 2 and 3 (Fig. 3) are *5mm* and the three balls placed below the holes in order to support the steel plate have a

diameter of *14mm*. The fourth hole pierced at the center of the plate allows applying a well known force always in a well-defined position. The diameter of the latter, *d=1mm*, is much smaller than the three previous ones in order to be neglected in the simulation.

On the other hand, as speckle techniques are used for displacements in the micrometer range, the material of the studied object must be quite stiff to induce weak slopes when the force is applied. That is why we decided to study a steel plate. Because we need a good accuracy in the results obtained by the finite element method, the Young modulus of the tested steel plate has been measured by the vibrational "resonalyser"[18] technique. This technique consists in supporting the test specimen by two thin wires to simulate the free-free boundary conditions of the FE-models as good as possible. The sample is excited with a computer controlled loud speaker using a white noise signal in the selected frequency range. The vibration response of the sample is measured with a laser Doppler vibrometer. The captured signal is digitised and stored into a computer. The resonant frequencies of the test specimen are extracted from the digitised time signals using an experimental modal analysis software. The material parameters are identified by minimising the differences between the experimental and numerical resonant frequencies in a least-squares sense. The Young's modules have been determined: E_X=2.26e+11 and E_Y=2.11e+11 N/m^2 quid de E_Z après tu donnes la valeurs utilisée d'ou sort elle ???.
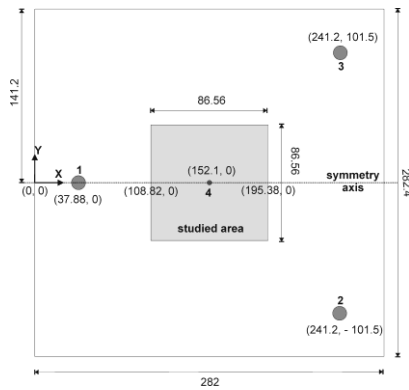

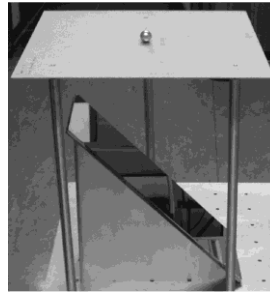
Fig. 3.a. Schematic of the studied steel plate.

Fig. 3.b. A photograph illustrating the central loading of a steel plate with a 12 g ball.

4. EXPERIMENT SIMULATION BY THE FINITE ELEMENT METHOD

In order to validate the measurement system, this experiment is simulated with the FEM software LAGAMINE, developed by M&S Department of the University of Liege[19]. The plate is modeled by eight-node mixed type volumetric brick elements with one integration point[20, 21]. Three layers of elements in the thickness are necessary to represent the bending phenomenon of the plate. The steel behaviour is described by an anisotropic elasto-plastic law based on HILL 48 yield locus. The Young's modules of the steel in three principle directions (Rolling Direction =X, Transverse Direction = Y and Thickness Direction= Z) are: E_X=2.26e+11, E_Y=2.11e+11 and E_Z= 2.185 N/m^2Ici tu parles du EZ donc il faut dire au dessus ou ici d'où il vient. Poisson's ratio is 0.254. The exact yield locus has not been measured as the strains clearly stay in the elastic range and follow Hooke's law.

Both the loading and the structure are symmetric with respect to the *X*- axis. While, only a half of the plate has been actually simulated. Fig. 4.a. shows the mesh for the whole plate to allow an easy comparison between the experiment and the simulations. In the zone scanned by the shearographic interferometer, a very fine mesh is chosen to increase the results accuracy as the displacements are non linear and that their derivatives will be compared to the shearographic measurements.

In the experiment, the plate is supported by three balls localized on three holes as explained in section 3. However in the numerical model, these three support balls are not described. Two configurations have been studied: the

plate with or without these three holes has been meshed and in each case one node from the bottom element layer of each hole or just located there has been fixed in three directions X,Y, Z (Fig. 4.a. and Fig. 4.b.).
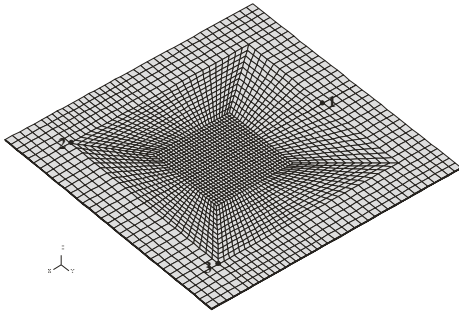

Fig. 4.a. Simulation with 3984 elements.
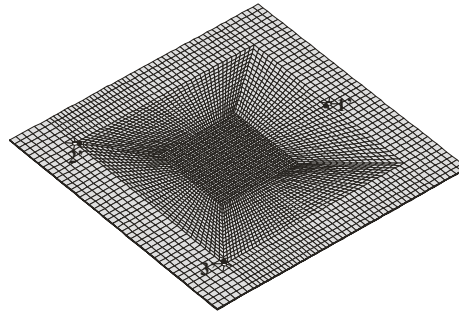The fixations are located at the points 1, 2, 3

Fig. 4.b. Simulation with 7365 elements.
The fixations are located at the points 1', 2', 3'

In the experiment, two moments have been pictured: the first one defines the plate position under its own weight and the second one determines the updated position after the loading by the ball of the 12g in middle of the plate. In the simulations, the ball is simplified as a concentrate force applied at the central node from the upper layer of the mesh. The initial shape of the plate is supposed to be perfectly plane which is of course not totally right. The simulations present two steps: in the first one the weight of the plate is applied and then, in the second one, the concentrated force is loaded. The nodal positions of those two moments are stored and their subtraction provides the displacement field due to the 12g ball.

Four simulations were performed. In the first approach, the plate was represented by a relatively coarse mesh (3984 elements, see Fig. 4.a.). The element size is 2.9x3.6mm^2 in the zone scanned by the shearographic interferometer. Two simulations were computed:

Simulation 1,   reference case: 3984 elements which did not described the three holes in the support points and measured Young moduli; the fixations are located at the coordinates of points 1, 2, 3 shown in Fig. 4.a.

Simulation 2,   to study the sensitivity of the support conditions: 4005 elements are now used with the three holes in support points; the fixations are located around.

In a second approach a refined mesh of 7344 elements is used to study the influence of mesh density. In the zone scanned by the shearographic interferometer, the element size is 2x2.7mm^2. With this new mesh, two additional simulations have been performed:

Simulation 3,   for studying the sensitivity of the mesh density: the new mesh without three holes in support points;

Simulation 4,   for studying the sensitivity of the support conditions: the new mesh with the three holes in support points; the fixations are located at the coordinates of points 1', 2', 3' shown in Fig. 4.b.

Fig. 5.a. shows the four curves of the displacements due to the 12g ball. As the experimental technique of shearography will provide, after numerical integration of the results, the displacement field relatively to the maximum displacement appearing at the loading point, the profiles of Fig. 5.a. also show the relative displacements.

Fig. 5.b. gives the four curves of displacement derivative relative to the X direction, $\partial w/\partial x$. The relationship used to calculate the derivatives will be described in the next section (Eq. 4).

In these figures, one can observe the sensitivity of the FEM results to the mesh density and to the support conditions. Each of these factors has an influence on the displacements and on their derivatives.
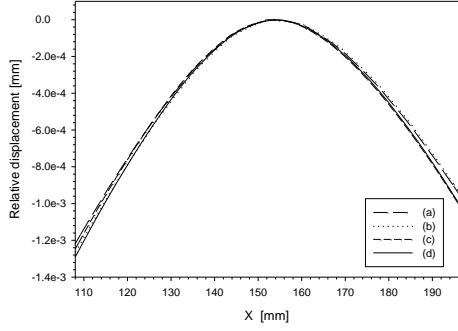
Fig. 5.a. Evolution of the profiles of the relative displacement w along the X axis and for the different simulations. (a) Simulation 1, without hole; (b) Simulation 2, with holes (c) Simulation 3, refined mesh without hole (d) Simulation 4, refined mesh with holes.
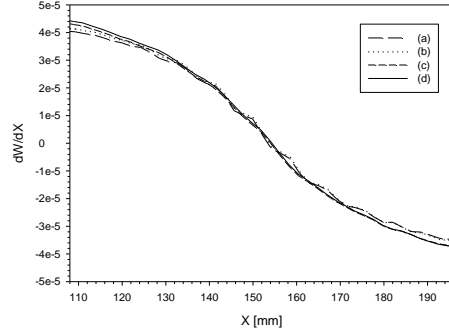
Fig. 5.b. Evolution of the profiles of the displacement derivative, $\partial w/\partial x$, along the X axis for the different simulations. (a) Simulation 1, without hole; (b) Simulation 2, with holes (c) Simulation 3, refined mesh without hole (d) Simulation 4, refined mesh with holes.

5. RESULTS AND DISCUSSION

The wrapped phase map, see Fig. 6.a, has been obtained with the four-buckets algorithm[13] applied to the phase shifted shearograms recorded for the steel plate before and after loading. The wrapped phase map of Fig. 6.a has been obtained with the experimental setup shown in Fig. 2 for a shearing amount of 8.4 mm, corresponding to a 0.35 mm thick glass plate, and the 12 g loading shown in Fig. 3.b. Before unwrapping the phase map, the noise has been reduced by filtering with a three dimensional mask at the sine/cosine level[14, 22, 23]. The filtered wrapped phase map is shown in Fig. 6.b and the corresponding unwrapped phase by the region growing technique[16] in Fig. 6.c. According to Eq. 2, the out-of-plane displacement derivative relative to the x direction, $\partial w/\partial x$, can be determined from the filtered and unwrapped phase map, Fig. 6.c; the quantitative results are presented in three dimensions in Fig. 7.
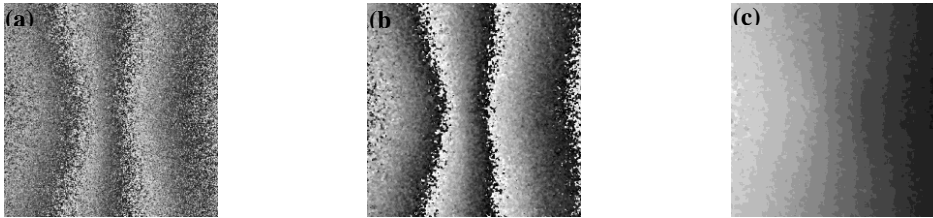

Fig. 6. (a) The wrapped phase map obtained with the shearographic interferometer illustrated in Fig. 2 and the loading illustrated in Fig. 3. The shearing amount, δx, is 8.4 mm. (b) The wrapped phase map of Fig. 6.a filtered once at the sine/cosine level by a mean mask of dimension three. (c) The phase map of Fig. 6.b unwrapped by the region growing technique.

The results obtained by shearography and by the finite element method cannot be directly compared. Indeed, the measurement obtained by shearography yields to the first derivative of the out-of-plane displacement relative to the shearing direction X, $\partial w/\partial x$, while the finite element method provides the out-of-plane displacement, w. In order to compare the results, either the displacement derivative obtained by shearography must be integrated relative to the

shearing direction X to obtain the displacement w or the out-of-plane displacement obtained by the finite element method must be derivated relative to the optical shearing direction X to numerically obtain $\partial w/\partial x$. In the following, both cases are discussed.

Fig. 8 presents the numerical out-of-plane displacement derivative relative to the optical shearing direction X, calculated from the displacement field w obtained by the numerical simulation. The numerical differentiation has been performed for each row of the displacement map, following this relationship:

$$\frac{\partial w(x)}{\partial x} = \frac{1}{2dx}\left[w\left(+dx\right) - w\left(-dx\right)\right] \qquad (4)$$

where $w(x)$ is the out-of-plane displacement of the material point relative to the xth pixel and dx is the sampling interval. However, the data representing the displacement field yielded by the simulation are not equally sampled because of the chosen mesh (Fig. 4.b, simulation 4). In order to use a constant sampling interval in the derivative calculation, the numerical displacements provided by the finite element method have been equally re-sampled by a local smoothing technique using a polynomial regression and weights computed from a Gaussian density function, performed thanks to the *Sigmaplot* software. Finally, the numerical differentiation have been computed with a sampling interval $dx=2mm$.

On the other hand, the experimental results obtained by shearography have been integrated relative to the X direction to obtain the out-of-plane displacement w. The numerical integration has been performed for each row following this relationship:

$$w(x) = \frac{1}{6}\sum_{i=0}^{x}\left[\frac{\partial w(i-dx)}{\partial x} + 4\frac{\partial w(i)}{\partial x} + \frac{\partial w(i+dx)}{\partial x}\right]dx \qquad (5)$$

where $\dfrac{\partial w(x)}{\partial x}$ is the out-of-plane displacement derivative of the material point relative to the xth pixel and dx is the sampling interval. In this case, the sampling interval has been chosen equal to the sampling of the steel plate image by the CMOS camera: $dx=0.29mm$.
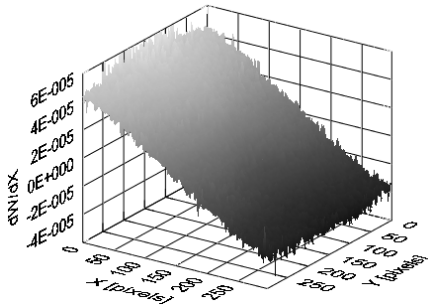

Fig. 7. The out-of-plane displacement derivative relative to the X direction, $\partial w/\partial x$, experimentally determined by shearography, from the unwrapped phase map of Fig. 6.c.
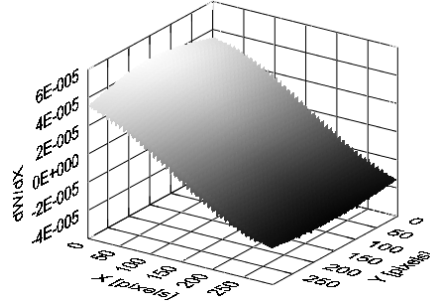
Fig. 8. The out-of-plane displacement derivative relative to the X direction, $\partial w/\partial x$, determined numerically by derivation of the displacement obtained by the finite element method (Fig. 5.a.).

In Fig. 7 and Fig. 8, the X and Y axis are presented in pixels but all represent exactly the same portion of the studied steel plate: the 300x300 pixels^2 correspond with the area scanned by the CMOS camera and represent an area of 86.56x86.56 mm^2 centered on the loading point of the steel plate (see Fig. 3.a).

A qualitative comparison of Fig. 7 and Fig. 8 can validate the experimental approach for the measurement of the first derivative of the displacement field relative to the optical shearing direction because those three dimensional representations present similar shape and the same order of magnitude, $\partial w/\partial x \approx 1e-4$ between two extreme points. In addition, the integration of the experimental results shown in Fig. 7 corresponds with a relative displacement field with

an order of magnitude, $w \approx 1\mu m$ (between the loading point and a point on the edge of the studied area), in agreement with the simulation 4 shown in Fig. 5.a.

However, a quantitative comparison between Fig. 7 and Fig. 8 shows that, even if the results are in very good agreement in most points, deviations reaching 20% can be observed mainly on the edge of the studied area. Those variations could arise from numerical processes like the sampling interval, the noise appearing from the numerical derivation,… but those numerical causes may be negligible compared to the errors on the experimental parameters encoded for the simulation by the finite element method: thickness of the steel plate, Young moduli, … Moreover, the steel plate is considered homogeneous and the physical parameters uniform, what may be slightly different in reality.

In order to better visualize quantitatively the differences between the results obtained by shearography and by the finite element method, profiles along the shearing direction X and passing by the loading point Y=0 have been extracted and superimposed, see Fig. 9 for the displacement profiles and Fig. 10 for the displacement derivative profiles. The continuous line of Fig. 9 and Fig. 10 represent respectively the displacement obtained by integrating the shearographic results and the displacement derivative measured by shearography while the dashed line represents the corresponding physical values obtained with the finite element method for the most advanced simulation, i.e. the simulation considering the holes and with a refined mesh (simulation 4, see Fig. 5.a and Fig. 5.b). We can see that the results are in good agreement. However, a greater difference between the experiment ant the simulation appears on the left edge of the studied area and can reach 18% at the coordinate X=108mm. We wanted to evaluate the influence of the Young moduli, E_X and E_Y on the simulation results. The latter have been measured by the resonalyser technique[18] that ensures the measurement value with an error of less than 1% [24]. However, a small variation in the thickness of the steel plate would also have a non negligible influence on the elastic sheet stiffness. To avoid a sensitivity analysis of the spatial thickness error, the simple approach of assuming a larger error on the Young moduli has been chosen. Finally an error of 5% on the Young moduli values has been applied. Consequently, elastic moduli reduced of 5% compared to the measured values have been used in the last simulation, the results are presented in dotted line in Fig. 9 and Fig. 10. The slight modification in the Young moduli has considerably improved the agreement between the simulation and the shearographic experimental results. The biggest differences between the continuous line corresponding to the results of shearography and the dotted line corresponding to the simulation with modified Young moduli are less than 3% for the out-of-plane displacement, w (see Fig. 9), and 12% for the out-of-plane displacement derivative, $\partial w/\partial x$ (see Fig. 10).
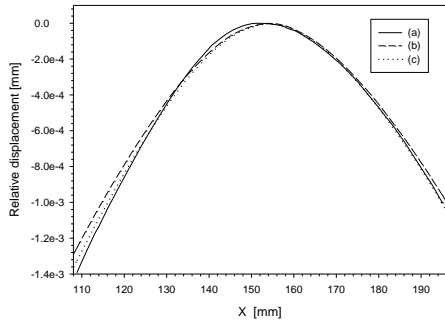

Fig. 9. Profiles of the relative displacement w along the X axis and passing by the loading point Y=0. (a) Integration of the out-of-plane displacement derivative obtained by shearography. (b) Simulation 4, with refined mesh and holes (idem Fig. 5.a, curve (d)). (c) Same as Fig. 9.b with Young moduli reduced of 5%.
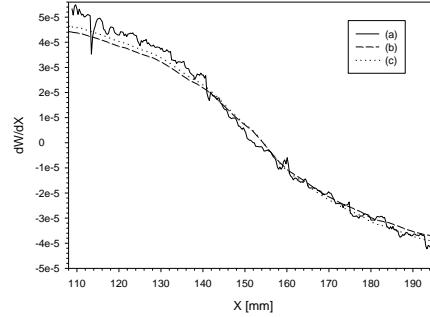
Fig. 10. Profiles of the displacement derivative $\partial w/\partial x$ along the X axis and passing by the loading point Y=0. (a) Out-of-plane displacement derivative obtained by shearography. (b) Derivative of the displacement obtained by the simulation 4, with refined mesh and holes. (c) Same as Fig. 10.b with Young moduli reduced of 5%.

6. CONCLUSION

An original experimental setup of shearography has been presented. The key element of the setup is the shearing device: a prism that separates the two polarization modes TE and TM thanks to a coating and a thin glass plate attached on its face. This shearing device and the use of components such as a CMOS camera and a liquid crystal variable retarder enable a compact, in-line and low-cost almost-common path experimental setup that is low sensitive to external disturbances. The efficiency of the shearographic experimental setup has been proved for the case of an out-of-plane displacement derivative measurement on a centrally loaded steel plate. This test has been simulated by the finite element method and the results of the computation have been compared with the measurements obtained by shearography. This comparison validated the efficiency of this shearographic interferometer for strain components measurement corresponding to displacements in the micrometer range. In this study, the efficiency of the experimental setup has been demonstrated in the particular case of the out-of-plane displacement gradient measurement but it can be easily extended to the in-plane displacement gradients measurement and, consequently, would find interesting applications in various emerging areas like non-destructive testing in electronics, mechanics or biomedical,…

REFERENCES

1. R. Jones and C. Wykes, *Holographic and Speckle Interferometry* (Cambridge U. Press, 1989).
2. P. K. Rastogi, *Digital Speckle Pattern Interferometry and Related Techniques* (John Wiley & Sons, Chichester, 2001).
3. W. Steinchen and L. Yang, *Digital Shearography* (SPIE Press, Bellingham, 2003).
4. Y. Renotte, D. Laboury, B. Tilkens, V. Moreau, and M. Morant, "At the crossing of Physics and Archeology : the OSIRIS Project (Optical Systems for Interferometric Relief Investigation and Scanning) - Development of a device for 3D numerical recording of archeological and epigraphic documents by optoelectronic processes," Europhysics News **35**(6), 205-207 (2004).
5. Y. Y. Hung, "A speckle-shearing interferometer: A tool for measuring derivatives of surface displacements," Optics Communications **11**(2), 132-135 (1974).
6. V. M. Murukeshan, O. L. Seng, and A. Asundi, "Polarization phase shifting shearography for optical metrological applications," Optics & Laser Technology **30**(8), 527-531 (1998).
7. Y. Y. Hung, "Applications of digital shearography for testing of composite structures," Composites Part B: Engineering **30**(7), 765-773 (1999).
8. H. M. Shang, Y. Y. Hung, W. D. Luo, and F. Chen, "Surface profiling using shearography," Optical Engineering **39**(1), 23-31 (2000).
9. R. M. Groves, S. W. James, and R. P. Tatam, "Shape and slope measurement by source displacement in shearography," Optics and Lasers in Engineering **41**(4), 621-634 (2004).
10. A. R. Ganesan, D. K. Sharma, and M. P. Kothiyal, "Universal digital speckle shearing interferometer," Applied Optics **27**(22), 4731-4734 (1988).
11. J. D. Valera and J. D. C. Jones, "Phase stepping in fiber-based speckle shearing interferometry," OPTICS LETTERS **19**(15), 1161-1163 (1994).

12. R. M. Groves, S. W. James, and R. P. Tatam, "Polarization-multiplexed and phase-stepped fibre optic shearography using laser wavelength modulation," Measurement Science and Technology **11**, 1389-1395 (2000).

13. K. Creath, "Phase-shifting speckle interferometry," Applied Optics **24**(18), 3053-3058 (1985).

14. D. C. Ghiglia and M. D. Pritt, *Two-Dimensional Phase Unwrapping: Theory, Algorithms, and Software* (John Wiley & Sons, New York, 1998).

15. T. J. Flynn, "Two-dimensional phase unwrapping with minimum weighted discontinuity," J. Opt. Soc. Am. A **14**(10), 2692-2701 (1997).

16. A. Baldi, "Phase unwrapping by region growing," Applied Optics **42**(14), 2498-2505 (2003).

17. N. A. Ochoa and J. M. Huntley, "Convenient method for calibrating nonlinear phase modulators for use in phase-shifting interferometry," Optical Engineering **37**(9), 2501-2505 (1998).

18. T. Lauwagie, H. Sol, G. Roebben, W. Heylen, Y. Shi, and O. Van der Biest, "Mixed numerical-experimental identification of elastic properties of orthotropic metal plates," NDT & E International **36**(7), 487-495 (2003).

19. S. Cescotto, A. M. Habraken, J. P. Radu, and R. Charlier, *LAGAMINE code preprocessor user's guide* (Ulg, BELGIUM).

20. L. Duchêne and A. M. Habraken, "Analysis of the sensitivity of FEM predictions to numerical parameters in deep drawing simulations," European Journal of Mechanics - A/Solids **24**, 614-629 (2005).

21. L. Duchêne, P. de Montleau, F. El Houdaigui, S. Bouvier, and A. M. Habraken, "Analysis of Texture Evolution and Hardening Behavior during Deep Drawing with an Improved Mixed Type FEM Element," in *Numisheet 2005*, L. M. Smith, F. Pourboghrat, J.-W. Yoon, and T. B. Stoughton, eds. (AIP Conference Proceedings, Proc. of the 6th Inter. Conf. and Workshop on Numerical Simulation of 3D Sheet Metal Forming Processes, 2005), pp. 409-414.

22. V. Rosso, F. Michel, V. Moreau, Y. Renotte, B. Tilkens, and Y. Lion, "Highlighting properties of filters for their application in temporal phase shifting interferometry," in *Photonic Applications in Biosensing and Imaging*, W. C. Chan, K. Yu, U. J. Krull, R. I. Hornsey, B. C. Wilson, and R. A. Weersink, eds. (Proc. SPIE 5969, 2005), pp. 626-635.

23. H. A. Aebischer and S. Waldner, "A simple and effective method for filtering speckle-interferometric phase fringe patterns," Optics Communications **162**(4-6), 205-210 (1999).

24. T. Lauwagie, H. Sol, and W. Heylen, "Handling uncertainties in mixed numerical experimental techniques," Journal of Sound and Vibration **291**(3-5), 723-739 (2006).